Spongelike metal surface generated by laser in the semiconfined configuration

Stjepan Lugomer[a) and Branka Mihaljević
Ruđer Bošković Institute, Bijenička c. 54, 10001 Zagreb, Croatia

Gabor Peto, Atilla L. Toth, and Eniko' Horvath
Research Institute for Technical Physics and Material Science, P.O. Box 49, H – 1525 Budapest, Hungary

A porous surface of tantalum and molybdenum plates has been formed by a nanosecond laser-matter interaction in the "semiconfined configuration," in which the laser plasma is trapped between the target and the transparent cover plate. The evolution of the plasma cloud and the pressure above the surface induce a superheated state in the liquid surface layer. Explosion of the plasma disk and formation of a cylindrical blast wave drive the superheated metastable fluid toward the spinodal, i.e., to the point of absolute thermodynamic instability. Phase explosion of a spinodal fluid occurs through the cascade of bubblings and generates a very porous spongelike surface $\sim 5-7$ μm thick (in some cases even ~ 10 μm), which stays frozen permanently because of ultrafast cooling at the end of the laser pulse. The total area of the porous surface is enlarged $\sim 10^4$ times at the microscale range. At even larger magnification, a different, nanoscale-type porosity has been observed. © *2005 American Institute of Physics*. [DOI: 10.1063/1.1884755]

I. INTRODUCTION

The technological importance of porous metals and metal surfaces is well known for catalysis and for chemical processing.[1,2] Among other technological applications one should mention electrolysis and electrochemical processes, applications to fuel cells, etc.[3] Recently, applications have emerged in dentistry and other medical fields, e.g., the joining of bone tissue and the implant surface.[4]

Difficulties in generating porous metal surfaces, especially of refractory metals, such as Ti, Ta, Mo, and W, are well known, since these metals have very high melting and boiling points, T_M and T_B, respectively. In the case of Mo, Ta, and W, T_B reaches 5000 K, a temperature that can hardly be reached by a classical production technology. Usually, sintering of metal powders is applied, as well as gaseous jets at elevated temperatures blowing through melted metals.

We show that porous, spongelike surfaces of Ta and Mo can be generated by nanosecond laser-matter interactions (nsLMIs) with high-power lasers, under special experimental conditions. Very porous metal surfaces are produced in laser ablation experiments performed in a special experimental configuration, which we call "semiconfined," in which a laser beam illuminates the target through a transparent cover plate positioned slightly above the target.

Laser ablation of solid materials has found applications in a growing number of areas ranging from deposition of materials (metal and dielectric films),[5,6] solid sampling for chemical analysis,[7,8] to ablative laser space propulsion.[9] This type of laser ablation has been performed in the "unconfined" configuration that makes possible free plasma expansion either in vacuum or in the low-pressure gaseous atmosphere from $\sim 10^{-2}$ to 10^{-3} Torr.[9,10] Many authors have

studied the ablation and the phase explosion (PE) from various aspects, i.e., for growing high-T_c superconducting thin films, for the study of deposition of particulates with respect to homogeneity of the film, the size and velocity distribution of atomized matter, and clusters and particulates emitted from metals and dielectrics. Singh *et al.*,[11] Bhattacharya *et al.*,[12] and Dyer *et al.*[13] studied surface superheating of yttrium barium copper oxide (YBCO) experimentally and theoretically. Their theoretical analysis was based on the solution of the one-dimensional (1D) heat-flow equation and on the postulation of the mass removal caused by subsurface superheating and explosive boiling.

Miotello and Kelly[14] argued against the boundary conditions used in Refs. 11 and 12 for the derivation of surface recession velocity and showed that the subsurface temperature gradient should be small.[15] They supported a model of explosive boiling based on a two-phase (liquid droplets vapor) system.[14] They showed that explosive boiling (PE) was associated with surface and not with the subsurface superheating. This model has been widely accepted, for example, it was utilized in recent work of Yoo *et al.*,[16] who studied PE in silicon.

Other types of laser ablation experiments are those performed in the "confined" configuration, in which the target surface is covered by a transparent plastic layer coated (deposited) directly on the surface. In this way laser plasma cannot expand in the space above the target, which generates a very large pressure shock. These experiments make possible the study of direction dependence of shock due to anisotropy in crystalline matter, of ultrafast large amplitude structural dynamics under high pressure, etc. Such a series of experiments was performed by Dlott.[17]

We have performed laser ablation experiments in the semiconfined configuration, in which the transparent cover plate is positioned slightly above the target surface. The ab-

a)Electronic mail: lugomer@rudjer.irb.hr

lated plasma has very limited space to expand, and is effectively trapped between the target surface and the cover plate. Since the expansion is prevented by the semiconfined configuration, the pressure increases driving the liquid surface layer into the superheated state, i.e., into the metastable liquid phase. At the moment when the plasma disk reaches the detonation threshold, explosion occurs, thus generating a quasi-two-dimensional (2D) blast wave.[18] The abrupt increase of pressure pushes the superheated liquid layer toward the spinodal (the point of absolute thermodynamic instability) and triggers the explosive phase transition of a spinodal fluid into the gaseous phase through the cascade of bubblings and bubble explosions.[14] Bubble explosions form porous, spongelike target surface morphology. This paper describes the result of such experiments.

II. EXPERIMENT

The experiments were performed using a single pulse of a Q-switched ruby laser ($E_s \sim 5$ J/cm^2, $P_s \sim 1.7 \times 10^8$ W/cm^2, $\tau = 30$ ns, $\lambda = 694$ nm) and by a Q-switched Nd:yttrium aluminum garnet (YAG) laser ($E_s \sim 10$ J/cm^2, $P_s \sim 2.5 \times 10^8$ W/cm^2, $\tau = 40$ ns, $\lambda = 1.06$ μm). Tantalum and molybdenum plates of $1 \times 1 \times 0.1$ cm^3, as very hard materials with high melting and boiling points, were used as targets. To generate conditions of very high temperature and pressure, the target was illuminated in the semiconfined configuration through a transparent quartz plate positioned slightly above the target surface.

III. RESULTS AND DISCUSSION

Surface morphology formed on the Ta target in the semiconfined configuration by a single pulse of a ruby laser is shown in Fig. 1. In contrast with the experiments in the unconfined configuration, the central circular crater has not been formed, only a visible spot because of ablation followed by the plasma explosion and the formation of a blast wave. The fingerprint of the plasma explosion associated with strong radial jetting is clearly seen. Radial jets, extending from the blast-wave envelope into the periphery region of the spot, are broken up into strings of drops as a result of the jet instability. The arrangement of drops in the strings is a regular one, while their size gradually decreases in the direction of the jet. This regular arrangement indicates that the greatest number of drops originates from the jet instability, and only a small part is ejected from the central part of the spot during the phase explosion. Since drops stay frozen-in on the surface, they make possible *a posteriori* study and precise measurements at large magnification.[19] The central part of the spot shows an unusual structure of deep surface porosity, as clearly seen in Fig. 2.

In contrast, the experiments performed in the unconfined configuration always result in the formation of a central crater with a slightly porous surface (Yoo *et al.*,[16] Pakhomov *et al.*,[9] Bhattacharya *et al.*,[12] Singh *et al.*,[11] and Miotello and Kelly.[14] Particulates and drops observed in these experiments are ejected in the free space above the target surface from the
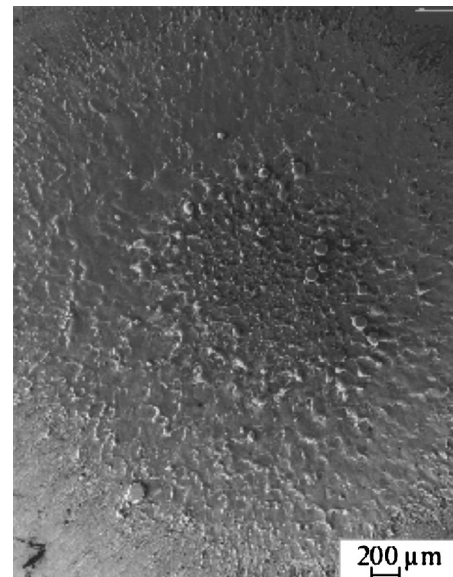

FIG. 1. SEM micrograph of the tantalum target after plasma explosion and formation of a blast wave caused by a Q-switched ruby laser in a "semiconfined" configuration. Notice that central crater has not been formed. Radial jetting extending from the blast-wave envelope is clearly seen. (Larger magnification of the periphery region reveals the breakup of jets into strings of drops. The greatest number of drops are regularly ordered in string formations, and only a small part ejected from the center of the spot is irregularly distributed.)

phase explosion in the center of the spot. Radial jetting and the jet instability resulting in the formation of a string of drops have not been observed.

A. Microscale morphology

1. Porous surface structures

The surface morphology in the center of the spot (Figs. 2 and 3) shows that smaller caverns are formed inside the larger ones through a series of bubble generation and explo-
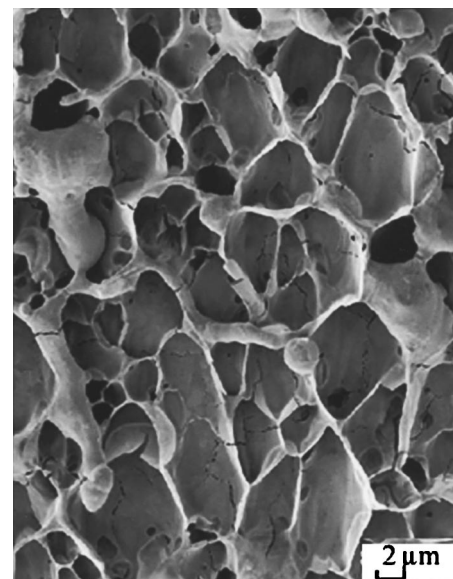

FIG. 2. SEM micrograph of the center of the spot showing porous surface formed by the phase explosion of a spinodal fluid generated by a Q-switched Nd:YAG laser on the tantalum target in a semiconfined configuration.
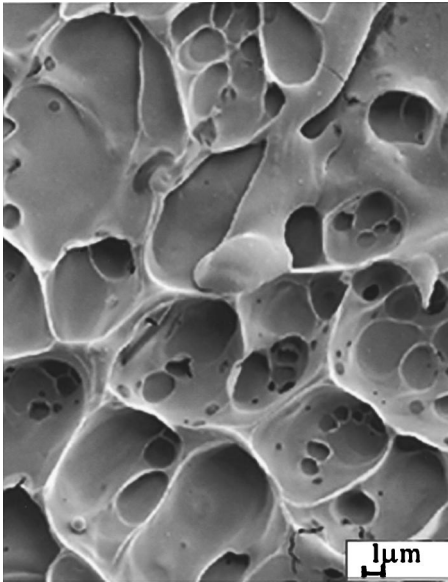
FIG. 3. SEM micrograph of the center of the spot showing microscale porous surface formed by the phase explosion of a spinodal fluid generated by *Q*-switched ruby laser on the molybdenum target in a semiconfined configuration.

sions. Three generations of bubbles (cascade) can be identified in micrographs. After the explosion of the first generation, a second generation of bubbles is formed inside caverns, and these also explode. The caverns formed on molybdenum targets irradiated by a Nd:YAG laser are of a nonequilibrium, irregular polyhedral shape (Fig. 2), whereas the caverns formed on tantalum targets irradiated by a ruby laser are of an equilibrium, rounded, almost spherical shape (Fig. 3). The structures with polyhedral bubble morphology of very thin walls are known as "dry foam," whereas the structures with spherical bubble morphology of thick walls are known as "wet foam" or froth.[20–22] This indicates that bubbling initiated by the Nd:YAG laser at high energy density starts in a fluid layer with the dominant vapor component, generating thin wall caverns; bubbling initiated by the ruby laser at lower energy density starts in a fluid layer with the dominant liquid component, generating thick wall caverns.

The cascade of bubble explosions forms a spongelike surface structure of Mo and Ta targets, which resembles a porous fractal structure called the Sierpínksi sponge.[23,24] The thickness of this three-dimensional porous structure reaches $5-7$ μm, but in some cases even ~ 10 μm. Since the average bubble radius is ~ 2.5 μm, and the bubble density ranges from $\sim 10^3$ to 10^4 in various samples, one finds that the porous surface of 1 cm^2 has a total area of ~ 1 m^2 (the area enlargement factor is 10^4); the equivalent expression is that the porous surface of 1 m^2 corresponds to a total area of $\sim 1-2$ football yards.

2. Formation of the plasma disk and superheated liquid surface

Strong ablation of tantalum and molybdenum causes the formation of a plasma cloud. Since the expansion of the plasma cloud in the semiconfined configuration is limited, it forms a disklike highly ionized plasma layer above the liquefied-boiling surface. The formation of the trapped plasma disk causes a large increase of pressure and a shift of the boiling point T_B to the higher temperature $T_{B'}$. The result is a reduced bubble nucleation rate, suppressed boiling, and surface superheating.

a. Surface superheating (metastable liquid surface). The metastable liquefied surface layer shows a very complex behavior. If the metastable phase is stable enough to sustain heterophase fluctuations during the laser pulse, the surface vaporization represents a basic mechanism of the phase transition, since the bubble nucleation is strongly reduced or absent.[15,16] Absorption of laser energy then causes the shift of the metastable phase closer to the point of absolute thermodynamic instability (spinodal). Difficulties in the theoretical analysis are connected with the problem of nonequilibrium phase transitions that have not been elucidated, especially the problem of behavior of the superheated metastable phase in the vicinity of absolute thermodynamic instability, because of singularity of thermodynamic functions.

In such a case, when surface vaporization represents the basic mechanism of the phase transition, the behavior of pressure $p[T(t)]$, which drives the superheated phase toward the spinodal, is described by the system of equations derived by Samohin,[25] and Samohin and Uspensky.[26]

To find the influence of the spinodal singularities on the behavior of the surface temperature $T_0(t)$, it is necessary to find the temperature profile in the metastable liquid taking into account the volume absorption of the laser energy, and the boundary condition on the vaporizing surface, which moves (with respect to the fixed liquid surface) with velocity $v(T_0)$. In the coordinate system with the origin at the vaporizing surface, the boundary condition for the heat conduction can be written[26] as

$$C_p\rho(\partial T/\partial t - v\rho_0/\rho\,\partial T/\partial x) - \partial/\partial x(\kappa\,\partial T/\partial x)$$

$$- C_p\rho(\partial T/\partial p)\,\partial p/\partial t = \alpha I \exp\left(-\int \alpha dx\right), \qquad (1)$$

$$\kappa T_0/\partial x = \varepsilon\rho_0 v, \ \ T(x,0) = T(\infty,t) = T_\infty, \qquad (2)$$

where I=laser intensity, while α, κ, ε, and $i\,C_p$ are the coefficients of absorption, of the heat conduction, of the heat of vaporization, and of the specific heat at constant pressure.[26] In the case of the free vaporization in vacuum, the vapor velocity v is given by[26]

$$v = (p_s\rho'/\rho_0\rho'_{\rm id})(m/2\pi KT_0)^{0.5}, \qquad (3)$$

where ρ_0 is the liquid density at the interface vapor/liquid, m=mass of the vaporizing particles, and $\rho_0/\rho'_{\rm id}$ indicates the difference between the vapor density ρ' and the density of the ideal gas $\rho_{\rm id}$ [at the temperature T_0 and the pressure $p_0(T_0)$]. The last term of the left side of Eq. (1) relates to the adiabatic change of temperature with the change of pressure p.[26]

Assuming the nonstationary regime of vaporization, and the absorption coefficient α=constant, one can also assume $\rho_0/\rho \sim 1$, in the convective term of Eq. (1). Then, introducing the nondimensional units[25,26]

$u = T/T_c$ (T_c = critical temperature), $\sigma = p/p_c$,

$\tau = \alpha^2 \chi_1 t$, $z = \alpha x$,

$D = I/\alpha \chi_1 T_c$, $g = \alpha \chi_1/v = \alpha \chi_1 (2\pi K T_c u/m)^{0.5}$,

$$\rho_0 \rho'_{id}/p_s \rho' = h \rho'_{id} \rho_0/\rho' \rho_i, \tag{4}$$

$\chi = \kappa/C_p \rho$ (thermal diffusion), h = function given below, Eq. (1) can be written[25,26] as

$$\partial u/\partial \tau - 1/g(\partial u/\partial z) - C_p \, \partial/\partial z (1/\kappa \, \partial u/\partial z) - (\partial u/\partial \sigma) \, \partial \sigma/\partial \tau$$

$$= C_p q \exp(-mz), \tag{5}$$

where m = parameter $\in [0,1]$, $q = mD$, $\partial u/\partial z|_0 = 0.81 \kappa/h$, with $u(o,z) = u(\tau, z_\infty) = u_\infty$. The functions g and h are given by[25,26]

$$g = h \exp(-1.3 u_0^5), \quad h = 10^{-3} u_0^{0.5} \exp[7.4(u_0^{-1} - 1)]. \tag{6}$$

In the case when the temperature of superheating depends on pressure, the specific heat and thermal conductivity become functions not only of temperature but also of pressure. The change of pressure is given by[25,26]

$$\sigma = p/p_c = 0.5[7.4(1 - u_0^{-1})]. \tag{7}$$

On the basis of the above relations, the singular behavior of the functions C_p and κ, approaching the spinodal, is described by the approximate expressions[25,26]

$$C_p = f^{1.2}, \quad \kappa = f^{0.66}, \tag{8}$$

where the function f is given by[25,26]

$$f = \{1 - \exp[-10^4(u_L - u)^4]\}^{0.25}, \tag{9}$$

where $u_L = (T_{eq} - T)/T_c$.

The functions C_p^{-1} and κ^{-1} are the approximate expressions of the singular behavior of the specific heat and thermal conductivity near the spinodal, respectively, while the function g/h describes the discrepancy of the real fluid with respect to the ideal one.[25,26]

The model predicts nonstationary vaporization with the oscillatory behavior of pressure.[27] The time scale of superheating and vaporization extending from the nanosecond to the microsecond time scale is somewhat too long for this experiment.

Since ionized vapor cannot expand freely in the semiconfined configuration, pressure increases abruptly and triggers the transformation of the superheated liquefied surface layer into a dielectric,[27,28] i.e., the inverse Mott transition. Thus, the superheated layer becomes transparent and makes possible a deep volume absorption of the laser beam. The vapor pressure above the surface that prevents boiling causes superheating of the whole heated volume. In the semiconfined configuration a large depth of ~ 10 μm was reached with the laser power density of only 10^8 W/cm^2 (determined from the thickness of the porous layer). For comparison, the equivalent depth in the unconfined configuration was reached at $\sim 10^{10}$ W/cm^2,[29] i.e., at a laser power density that is higher by two orders of magnitude (on the silicon target that has T_B of ~ 2638 K or about 2500 deg lower boiling temperature than tantalum and molybdenum).

b. Blast-wave generation by the plasma-disk explosion. The plasma cloud above the target surface becomes highly ion-

ized and highly absorptive. The absorption of laser energy continues to the plasma explosion, which generates a blast wave whose evolution dynamics and geometry depend on the distance between the target surface and the transparent cover plate. If the cover plate is positioned a few millimeters or centimeters above the target, the blast-wave geometry is hemispherical (spherical), just as in the case of unconfined configuration.[30,31]

The radius R of the spherical blast wave is described by the Taylor–Sedov relation[18,30–32]

$$R = C(E_p/\rho)^{1/5} t^{2/5}, \tag{10}$$

where E_p is the energy that drives the plasma explosion and ρ is the density. The (E_p/ρ) may be written as (Zeldowich and Raizer[18] and Grun *et al.*[30])

$$E_p/\rho = \{[75(\gamma-1)(\gamma+1)^2]/[16\pi(3\gamma-1)\rho_0]\}^{1/5}, \tag{11}$$

where γ is the adiabatic coefficient of the plasma gas, and C is a constant, usually $C \sim 1$.[30] If the cover plate is located about $1-2$ mm above the surface, the geometry of the blast-wave evolution is spheroidal, or better, the oblate spheroid.

However, if the transparent cover plate is positioned a few tens or hundreds of micrometers above the target, the blast wave is formed in a semiconfined configuration with the limited possibility for evolution. In this configuration, the blast wave evolves into a cylindrical slab, the radius of which is also described by the Taylor–Sedov relation for cylindrical geometry,[18,32]

$$R = C(E_p/\rho)^{1/4} t^{1/5} \tag{12}$$

or in the extended form[32]

$$R = \{[4(\gamma-1)(\gamma+1)^2]/[\pi(3\gamma-1)]\}^{1/4}(E/\rho)^{1/4} t^{1/2}, \tag{13}$$

where $E(J)$ is the laser energy deposited in the spot. Assuming that the blast-wave expansion occurs in $t \sim 20$ ns, assuming $\rho \sim 1$(kg/m^3), and the coefficient of adiabatic expansion, $\gamma = 1.4$, one finds for the blast-wave radius from Eq. (13), $R \sim 2600$ μm, in good agreement with the measured value $R \sim 2850$ μm. (Fig. 1). The supersonic blast wave travels at a velocity of $\sim 10^6$ cm/s and increases the pressure up to ~ 30 kbar $\sim (30 \times 10^3$ atmospheres)—roughly estimated on the literature basis.[16,32]

3. Spinodal explosion of a liquefied surface layer

The very high peak pressure generated by the blast wave drives the metastable layer to the spinodal, i.e., to the point of absolute thermodynamic instability. The transition from the superheated, metastable liquid phase into the gaseous phase is described by van der Waals equations. These equations form the "cusp catastrophe," with temperature and pressure as the conflicting control parameters and with density as the behavior axis. In the usual representation of the cusp catastrophe, the top sheet is the liquid phase and the bottom sheet is the gaseous phase: the two catastrophes are boiling and condensation. The vertex of the cusp is the critical point at which liquid and gas exist simultaneously.[33,34]

The calculations of Grosse[35] have shown that superheating may in principle occur for all metals, but that the spinodal curve for some of them is flat rather than cusplike.
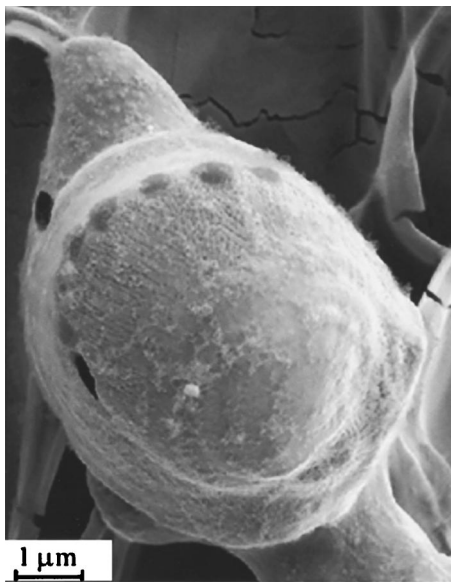
FIG. 4. SEM micrograph of the porous surface of the Mo target made by a Q-switched Nd:YAG laser showing details of the structure. A regular arrangement of circular holes is observed on the circumference of a droplet-like object, the origin of which is not known.

However, for refractory metals (Ti, Ta, Mo, W, ...,) the cusp is large, and superheating may reach even $10^3 - 10^4$ K. At the spinodal, the system is in the region of absolute thermodynamic instability, where the thermal conductivity $\kappa \to 0$ and the specific heat $C_p \to \infty$.[35] Fluctuation, which plays a crucial role, triggers the transition from superheated spinodal fluid into vapor through abrupt homogenous bubble nucleation and PE.

The deep phase explosion of the spinodal fluid down to ~ 10 μm into the surface indicates a transition from "planar" to "volume" boiling, which is not a well-elucidated problem from the aspect of the phase diagram or from the aspect of surface dynamics and the corresponding morphology. Ultrafast cooling at the rate $>10^9$ K/s associated with the pulse termination causes that surface morphology comprising caverns stays frozen permanently, thus making possible *a posteriori* study.

B. Nanoscale morphology

1. Nanoaggregates

The scanning electron microscopy (SEM) analysis of a porous target surface does not indicate the existence of large clusters or particulates after backward reflection from the cover plate. The nanoscale aggregates of condensed monoatomic vapor of $\sim 100 - 200$ nm in size at the surface of microscale caverns can be seen in Fig. 4. Some of the aggregates are dense compact structures with chainlike or closed-loop segments, formed by condensation from the vapor phase.

On the other hand, the PE in the unconfined configuration, in which the laser beam directly illuminates the target (in vacuum or in the low-pressure atmosphere), ejects large clusters (~ 100 nm) and particulates ($\geqslant 100$ nm), in addition to atomized target species, as observed by mass-spectrometric studies.[36,37] The time-resolved measurements

performed by Geohean,[10] Lu *et al.*,[29] and Pakhomov *et al.*[9] have shown that monoatomic species have a relatively small velocity $\sim 200 - 500$ m/s, whereas clusters and particulates reach an ~ 10 times higher velocity of $\sim 1 - 6$ km/s.[9] The existence of clusters and particulates, in addition to monoatomic vapor of the ablated material, requires a few different models of condensation appropriate for every type of particles, thus complicating the interpretation of data.[9] Ddupendent *et al.*,[38] who studied the particulate formation from Al, Cu, Fe, Y, ..., targets, noticed that Al and Y demonstrated much higher particulate density compared with Fe, Cu, and Au. They could not find a correlation with the thermal properties of these elements either.

The formation of nanoaggregates from laser ablation is a phenomenon observed in many cases,[23] but still not completely understood. As pointed out by Anisimov and Luk'yanchuk,[27] we are dealing with the kinetics of ultrafast phase transformation of the first order, and the cooling rates in the vapor expansion that reach $10^{10} - 10^{11}$ K/s, the rate not very common in classical physics, and a strongly nonlinear phenomenon. Since the experiments are very difficult to perform, the theoretical modeling (analysis) of condensation dynamics is based on the work of Raizer[28] and Zeldowich and Raizer,[18] who developed the theory of ultrafast condensation of expanding vapor (ZR theory). In the case of a two-phase vapor-liquid system, free of large clusters and particulates, a single model of condensation is appropriate for the description of redeposited material on the target surface.[27]

Based on the first-order phase transition, the ZR theory introduces the "supercooling parameter"[27]

$$\theta = (T_{eq} - T)/T_{eq}, \tag{14}$$

as the main parameter in dynamic vapor condensation, the scenario of which comprises two steps: (i) formation of critical nuclei in the vapor phase and (ii) growth of supercritical nuclei. In the above relation, T=vapor temperature, and T_{eq} is the equilibrium temperature along the binodal.[27]

Omitting the complex mathematical treatment and theoretical aspects (see Ref. 27), we briefly summarize the process from the phenomenological point of view. The process of dynamical vapor condensation is associated with three types of waves simultaneously propagating from the periphery to the center of the spot:[27]

(a) the vapor saturation wave,
(b) the wave of nuclei injection (the critical nuclei are injected into the saturation vapor at the instant of time when supercooling reaches maximum),
(c) the vapor quenching wave (the particle collisions in vapor terminate at some stage of the process).

For a plausible interpretation, we adopt this ZR scenario without specific details which are not yet clear even for the "open configuration" experiments. We concentrate on the characteristics of nanoaggregates that can be determined from micrographs (see Figs. 5–7).

Visual inspection indicates that nanoaggregates adsorbed on the convex and concave parts of the porous surface are self-similar fractal structures, very similar to diffusion-limited aggregates (DLAs). In this process, the monomers
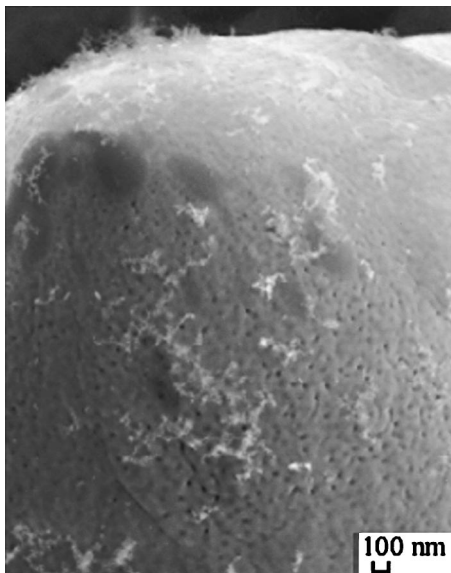
FIG. 5. SEM micrograph showing a fine structure of nanoaggregates of ~100–150 nm in size, redeposited by ultrafast condensation from the vapor phase.

FIG. 7. SEM micrograph at very large magnification shows 3D aggregates on tilted molybdenum sample.

start from far away and diffuse by a random-walk process (Brownian trajectory). The wandering monomers stick to the growing aggregate when they reach it. The fractal dimension, which is the measure of how the aggregate fills the space it occupies, is determined from the correlation function $C(r)$,[23,24]

$$C(r) \sim r^{D-d}, \tag{15}$$

where D is the Euclidean dimension ($D=2$) and d is the fractal dimension of the aggregate. By using the standard box counting method on a few aggregates, it was found that $d=1.73-1.76$, in good agreement with the prediction of the DLA model $d=1.75$.[23,24]

FIG. 6. SEM micrograph showing a fine nanoscale structure of a tilted molybdenum sample. A 3D structure of nanoaggregates resembles the fractal DLA and CCA clusters. Notice that large clusters and particulates are not present in this case.
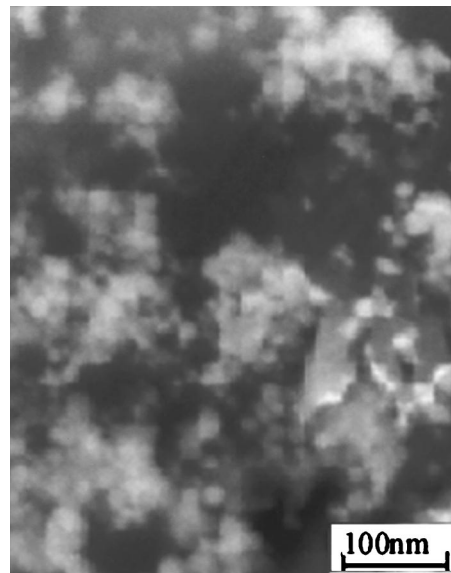
Another type of aggregates are chainlike, compact closed-loop structures, the larger magnification of which reveals the similarity with cluster-cluster aggregates (CCAs), described by the Meakin–Julien model.[39] This model not only describes the chain-aggregate growth but also explains the chain-aggregate compactification. This two-step model comprises diffusion in the first step, and readjustment of the structure in the second step. Readjustment by one rotation does not lead to the formation of a loop, while the readjustment by two rotations leads to the true loop, thus increasing the local aggregate compactification. This model shows that both the Brownian and linear trajectories result in the local compactification on length scales of a few particle diameters. The compactification increases further with the presence of the two rotations in the second step.[39] Depending on the diffusion mechanism (step 1) and the rearrangement (step 2), the fractal dimension calculated from the model is ~1.55,[39] which is somewhat lower than that found from the micrograph, $d=1.58-1.60$.

Therefore, the effects of the chain mobility result in aggregates becoming considerably more compact on a very short-range scale, whereas the fractal dimension which characterizes their structure on a large length scale is increased only slightly.[39]

The SEM analysis of tilted samples reveals that all aggregates are three-dimensional (3D) objects. Figures 6–8 show that the shape and size of these aggregates are very similar to 3D aggregates of CCA of colloidal gold, as reported by Weitz and Huang,[40] Feder,[23] and Carriere *et al.*,[41] but also to aggregates of iron, zinc, and nickel, as well as to aggregates of Ta oxide.[42,43] The nsLMIs do not offer the possibility of *in situ* studying the growth of 3D aggregates; however, we estimate their fractal dimension to be in the range of $d \sim 2.2-2.5$, in agreement with the dimension of DLAs and CCAs reported in the literature.
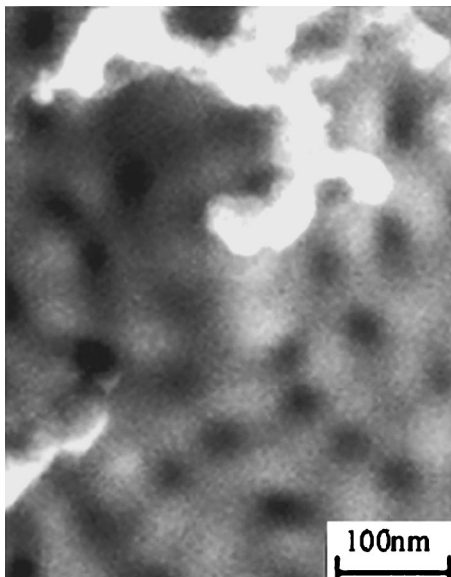
FIG. 8. SEM micrograph showing a fine nanoscale structure of a tilted molybdenum sample. Very large magnification reveals nanoholes of ~20–30 nm in diameter.

2. Nanoholes

The "convex" parts of the porous surface—in addition to the above DLAs and CCAs—comprise almost regularly distributed circular holes of a diameter ranging from ~25 to 30 nm. (see Fig. 8). The study of these surfaces in the tilted position at large magnification by the stereo scan EM has shown nanoholes. Spontaneously formed, the nanoholes extend into the surface, thus generating porosity at even smaller scale. At present their origin in nsLMI is not clear and requires further study.

IV. CONCLUSION

We have demonstrated that the "semiconfined" configuration of nsLMI is a very practical and promising method for generating spongelike metal surfaces, including metals with the highest melting and boiling points. The surface porosity formed by explosion of spinodal fluid gives the total area ~10^4 times larger than the smooth surface, a factor very large and interesting for various technological applications.

The LMI in the semiconfined configuration causes surface superheating and the dielectric transition makes the superheated surface transparent, thus making possible deep penetration of the laser beam. The blast-wave formation by the plasma explosion causes a high dynamic pressure which pushes the superheated surface layer to the point of absolute thermodynamic instability, triggering the phase explosion and transition into the vapor phase.

From the fundamental point of view, these experiments show that the transition from the superheated liquid metal at (or near) the spinodal into the stable vapor phase occurs in a cascade rather than in a single jump; the spongelike tantalum and molybdenum surface is a consequence of the cascade bubble explosions that belong to the class of phase explosion phenomena.

In addition, these processes cause some other nanoscale phenomena:

(i)   redeposition of monoatomic vapor and formation of 3D aggregates which strongly resemble fractal DLA or CCA clusters and

(ii)   formation of nanoholes on spherical surfaces, the origin of which is not presently clear and requires further study.

The LMI experiments in a semiconfined configuration performed on various target materials offer the possibility of studying spinodal fluid behavior, the cascade transition from the metastable to the stable vapor phase, and the ultrafast dynamic condensation of vapor into nanoaggregates, the problems which in nsLMIs are not yet completely understood.

[1] www.stormingmedia.us/cgi-bin/keywords.porous metals
www.mri.psu.edu/conferences/sint03/pdf/myers_3_10.pdf
www.metalfoam.net/commercial.html
[2] V. Sotirchos and V. Burganos, MRS Bull. **24**, 41 (1999).
[3] S. Morooka and K. Kusakaki, MRS Bull. **24**, 25 (1999).
[4] G. Pezo, A. Karaks, Z. Paszti, L. Guczi, T. Divinyo, and A. Joob, Appl. Surf. Sci. **186**, 7 (2002); www.medicine.com/orthoped/topic610.htm
[5] K. B. Erington, W. McGahan, N. J. Ianno, and J. A. Wollam, in *Laser Ablation for Materials Synthesis*, edited by D. C. Paine and J. C. Brawman (MRS, Pittsburg, PA, 1990), p. 97.
[6] K. B. Erington and N. J. Ianno, in *Laser Ablation for Materials Synthesis*, edited by D. C. Paine and J. C. Brawman (MRS, Pittsburg, PA, 1990), p. 115.
[7] M. A. Shanon, X. L. Mao, A. Fernandez, W. T. Chan, and R. E. Russo, Anal. Chem. **67**, 4522 (1995).
[8] A. Fernandez, X. L. Mao, W. T. Chan, M. A. Shanon, and R. E. Russo, Anal. Chem. **67**, 2444 (1995).
[9] A. V. Pakhomov, M. S. Thomson, and D. A. Gregory, J. Phys. D **36**, 2067 (2003).
[10] D. B. Geohean, Appl. Phys. Lett. **62**, 1463 (1993).
[11] R. K. Singh, D. Bhattacharya, and J. Narayan, Appl. Phys. Lett. **57**, 2022 (1990).
[12] D. Bhattacharya, R. K. Singh, and P. Holloway, J. Appl. Phys. **60**, 1890 (1992).
[13] P. E. Dyer, S. R. Farer, and P. H. Kelly, Appl. Surf. Sci. **54**, 255 (1992).
[14] A. Miotello and R. Kelly, Appl. Phys. Lett. **67**, 3537 (1995).
[15] A. Miotello (private communication).
[16] J. H. Yoo, S. H. Jeong, R. Greif, and R. E. Russo, J. Appl. Phys. **88**, 1638 (2000).
[17] D. D. Dlott, Acc. Chem. Res. **33**, 37 (2000).
[18] Y. B. Zeldovich and Y. P. Raizer, *Physics of Shock Waves and High-Temperature Hydrodynamic Phenomena* (Academic, New York, 1966).
[19] S. Lugomer *et al.* (unpublished).
[20] S. R. K. Masurvada and C. W. Park, Phys. Fluids **8**, 3229 (1996).
[21] H. K. Tsao and D. L. Koch, Phys. Fluids **9**, 44 (1997).
[22] A. K. Chesters and G. Hofman, Appl. Sci. Res. **38**, 353 (1982).
[23] J. Feder, *Fractals* (Plenum, New York, 1988).
[24] T. A. Witten and L. M. Sander, Phys. Rev. B **27**, 5686 (1983); T. Vicsek, Phys. Rev. Lett. **53**, 2281 (1984); L. M. Sander, Nature (London) **322**, 789 (1986); M. Barnsley, *Fractals Everywhere* (Academic, New York, 1988).
[25] A. A. Samohin, in *Absorption of Laser Radiation in Condensed Matter*, edited by Fedorov (Trudi IOFAN, Academy of Sciences of USSR, 1988), p. 38.
[26] A. A. Samohin and A. B. Uspensky, Zh. Eksp. Teor. Fiz. **73**, 1025 (1977).
[27] S. I. Anisimov and B. S. Luk'yanchuk, Phys. Usp. **45**, 293 (2002).
[28] Y. P. Raizer, Sov. Phys. JETP **10**, 1226 (1960).
[29] Q. Lu, S. S. Mao, X. Mao, and R. E. Russo, Appl. Phys. Lett. **80**, 3072 (2002).
[30] J. Grun, J. Stamper, C. Manaka, J. Resnick, J. Craford, and B. H. Ripin, Phys. Rev. Lett. **66**, 2738 (1991).
[31] S. S. Mao, X. Mao, R. Greif, and R. E. Russo, J. Appl. Phys. **89**, 4096 (2001).
[32] D. C. Lobao and A. Povitsky (unpublished).
[33] E. C. Zeeman, *Catastrophe Theory* (Addison-Wesley, Reading, MA, 1977).

[34]T. Poston and I. Stuart, *Catastrophe Theory and Its Applications* (Pitman, London, 1978).

[35]A. V. Grosse, J. Inorg. Nucl. Chem. **22**, 23 (1961).

[36]C. H. Beker and J. B. Palix, J. Appl. Phys. **64**, 5152 (1988).

[37]O. Eryn, Appl. Phys. Lett. **54**, 2717 (1989).

[38]H. Ddupendent, J. P. Garigan, D. Givord, A. Lienard, J. P. Rebouillat, and Y. Sauche, Appl. Surf. Sci. **43**, 369 (1989).

[39]P. Meakin and R. Julien, J. Phys. (France) **46**, 1543 (1985).

[40]D. A. Weitz and J. S. Huang, in *Aggregation Gelation*, edited by F. Family and D. P. Landau (North-Holland, Amsterdam, 1984), p. 19.

[41]T. Carriere, C. Ortiz, and G. Fuchs, J. Appl. Phys. **70**, 5063 (1991).

[42]S. Lugomer, Vacuum **45**, 871 (1994).

[43]S. Lugomer, *Laser-Matter Interactions: Surface Self-Organization* (Profil International, Zagreb, 2001).